Investigating the Effects of MDH2 Mutations: G37R, P133L, and P207L Kill Enzyme Activity *in Vitro*

Amber Murphy

Dr. Kathryn Huisinga, PhD

Malone University

April 24, 2020

Abstract

The mitochondrial malate dehydrogenase (MDH) enzyme converts malate to oxaloacetate as part of the Krebs Cycle. Clinical studies identified three male patients with severe encephalopathy who carried bi-allelic mutations in the human MDH2 gene (Ait-El-Mkadem). These mutations included Gly37 to Arginine, Pro133 to Leucine, and Pro207 to Leucine. Gly37 is located in the NAD binding pocket, Pro133 is located in a turn between an α helix and a β strand, and Pro207 is located in a β strand. It was hypothesized that these MDH2 mutations would affect the stability of the protein. The enzymatic activity of recombinant human MDH2 containing single mutations in Gly37, Pro133, and Pro207 were examined against the wild type *in vitro* to determine K_m and V_{max} values. First, specific activity was determined. If a substantial specific activity was found, then oxaloacetate and NADH were titrated separately across a range of concentrations as the reaction was monitored. Only the wild type was found to have a significant amount of enzymatic activity, so the assays titrating oxaloacetate and NADH were never performed on the mutants. The results from these investigations demonstrate that the G37R, P133L and P207L significantly diminish enzyme activity *in vitro*.

Table of Contents

Introduction

Enzymes are biomolecules, generally proteins, that act as catalysts. They help to regulate the speed of chemical reactions by binding a desired substrate and accelerating the reaction that converts the substrate into product. Mitochondrial malate dehydrogenase (MDH2) is the isoenzyme that catalyzes the conversion of malate and NAD^+ to oxaloacetate and NADH as part of the Krebs Cycle (Fig. 1A). The Kreb's Cycle is the process by which most living cells oxidize carbon to generate reduced electron carriers during aerobic respiration. It takes place in the mitochondrial matrix, and the electron carriers generated may move on to other pathways such as oxidative phosphorylation in order to generate ATP (sigmaaldrich). If enzyme activity is reduced, some of the chemical reactions that take place in the body would occur too slowly. This would cause a buildup of intermediates, and metabolic pathways such as the Krebs Cycle would not be able to be sustained.

Mitochondrial diseases stemming from disruptions in the respiratory chain manifest themselves in many different ways. These disruptions may cause respiratory issues, motor deficits, and certain cancers (Cascon). Mutations in the Krebs Cycle are frequently found in patients with paragangliomas/cancer. Disruptions in enzyme activity caused by these mutations lead to an accumulation of certain metabolites such as fumarate and succinate. Eventually, this buildup could halt the cycle altogether leading to a buildup of acetyl-CoA. These disruptions slow down ATP production and give rise to epigenetic changes in the genome that cause a hypermethylated phenotype, which is characteristic of a loss in tumor suppressing genes. In other words, the significant lack of ATP has major consequences on the individual's metabolism because energy is not being produced to keep the body running properly. Therefore, the

hypermethylated phenotype is extremely deadly because once a cancer ultimately arises due to any irreparable damages caused by DNA mutations, the entire system will shut down, and the individual will die (Remacha).

The most significant organ that tends to be affected by disruptions in the Krebs cycle is the brain (Ait-El-Mkadem). However, these diseases are extremely rare. Genetic diagnosis and treatment of these disorders is incredibly challenging because there is a substantial lack of information. Due to the complex cellular systems involving metabolism and the mitochondrial matrix, such as the Krebs Cycle, these diseases are extremely diverse and pleiotropic. As a result, they are extremely challenging to study and research (Lasserre).

Recent clinical studies have identified certain mutations in MDH2 linked to the onset of encephalopathy, or neurological disorders, in humans (Ait-El-Mkadem). Some studies have used oxidative phosphorylation spectrophotometric measurements, muscle histopathology and ultrastructure, mitochondrial DNA molecular analysis, and cell cultures as probative techniques (Rouzier). However, they have not looked into enzyme kinetics. Related studies have used enzyme kinetics to study similar enzymes found in the cytoplasm of yeast or watermelon glyoxysomal MDH (Hock).

A clinical study performed in 2016 identified mutations in the mitochondrial version of MDH2 linked to the onset of encephalopathy, or neurological disorders. Three unrelated male individuals who displayed hypotonia and seizures at an early age were investigated, and three different MDH2 point mutations were identified that mapped to the following amino acids: Glycine 37 to Arginine, Proline 133 to Leucine, and Proline 207 to Leucine. Gly37 is located in the NAD binding pocket; Pro133 is located in a turn between an α-helix and a β-strand; and

Pro207 is located in a β-strand (Fig. 2). It was hypothesized that these variations in each of these subjects would affect the stability of the protein. Western blotting showed that MDH2 levels were not detectable in subjects 1 or 2, which supports the hypothesis that MDH2 mutations affect protein stability. Enzymatic activity was notably decreased evidenced by a significant MDH deficiency (Ait-El-Mkadem).

However, because each of the individuals in the study had both copies of the MDH2 gene disrupted, it is unclear which of the mutations affect protein stability. It is feasible that any one of the single mutations could disrupt the conversion of malate to oxaloacetate due to the high specificity of binding in the human body. Glycine is a nonpolar, aliphatic R group consisting of a single Hydrogen. A mutation to Arginine causes this R group to become a positively charged R group that is significantly larger. Proline is a nonpolar, aliphatic R group as well. While a mutation to Leucine does not affect charge, it does significantly affect the size and structure of what normally would be found on human MDH2 (Fig. 3).

To investigate the effect of each individual point mutant on MDH enzymatic activity, the K_m, V_{max}, and K_{cat} of wild type MDH2 was experimentally determined. Cultures containing each mutation and the wild type were grown to a proper optical density, and the His-tagged proteins were induced with IPTG to optimize protein expression (Fig. 4). Each mutation was then purified and separately tested for any activity. Specifically, Glycine 37 to Arginine, Proline 133 to Leucine, and Proline 207 to Leucine mutants have been tested for their enzymatic activity compared to the wild type. Based on the locations of Pro133 and Pro207, these mutations to Leucine were predicted to alter the structural integrity of the MDH2, resulting in destabilization of protein regions necessary for functional protein folding. Therefore, enzyme activity would be

diminished. The Gly37 mutation to Arginine was predicted to diminish activity as well since the binding of NAD^+ is likely disrupted. If NAD^+ is not able to properly bind, there will be little to no NADH generated as a byproduct of the reaction.

Materials and Methods

Gly37 was mutated to Arginine; Pro133 was mutated to Leucine; and Pro207 was mutated to Leucine. These mutations were completed via site-directed mutagenesis in the Spring of 2018, and freezer stocks were made for future use. Fresh LB media plates with 50ug/mL Kanamycin were poured, and they were streaked with plasmids from freezer stock BL21 cells. The plasmids all carried an antibiotic resistant gene and were grown up in *E. coli*. Once growth was achieved, liquid 10mL cultures were obtained for each sample by inoculating sterile LB media with a single colony. The cultures were grown to an OD_{650} of about 0.5, expanded to larger 250mL cultures, and again monitored to an OD_{650} of about 0.5. Once this optical density was achieved, each culture was induced with 147.8 µL of IPTG for a final concentration of 0.5 mM IPTG. Multiple investigations were completed, and 2 sets of each sample were induced at 37°C for 4 hours while in a shaker to stimulate growth. One set of each sample was induced at 25°C for 20 hours while in a shaker to stimulate growth. These different induction conditions were used to optimize expression of the protein. Moving forward, the samples induced at 37°C were used because it more closely resembles internal body temperature.

To ensure that the desired protein had been induced, cell samples pre and post induction were run on a 12% bis-acrylamide SDS-PAGE gel. Afterwards, cells were resuspended in 10mL of PBS. 100 µL of 100 mM PMSF for a final concentration of 1 mM, 7 µL of 14 M β-(2-)mercaptoethanol for a final concentration of 10 mM, and about 0.01 g of Lysozyme for a

final concentration of 1 mg/mL were added to each sample. The cells were incubated on ice as they were lysed. A 6.25mL aliquot of Ni-NTA resin beads was prepared for each sample by transferring 12.5 mL of a 50% slurry of beads equilibrated into a clean tube for each. The lysate was then added to each tube containing resin along with one resin bed volume (6.25 mL) of His-Binding buffer. Two resin bed volumes (12.5 mL) of His-Wash buffer (20 mM Imidazole) was used to wash the nickel resin added to the induced cell pellets for contamination and unbound protein. This was done until absorbency at 280 nm reached baseline (four washes for each sample). One resin bed volume (6.25 mL) of His-Elution buffer (300 mM Imidazole) was used to elute the His-tagged proteins from the resin so they could be used for enzyme assays. This was also done until absorbency at 280 nm reached baseline (four washes for each sample) (Fig. 4).

After column purification, each sample was run in a 12% SDS-Page gel to determine which fractions contained protein. A 1X SDS-PAGE running buffer was used, and a 4X SDS-PAGE gel loading buffer was added to each sample to load into the gel. Before being run in the gel, each sample was heated at 95^{o}C for 5 minutes to carefully denature the proteins and placed in an ice bucket for 1 minute to cool them. 10 μL of each sample was loaded into the gels, and each gel was run for about 1 hour. The gels were removed and covered with Coomassie Blue R-250 inside a plastic lid and placed on a shaker until the markers were visibly stained. They were then placed in a destaining solution and placed back on the shaker to destain overnight.

As an extra measure to verify protein in each of the elutions, quick Bradford assays were performed for each of the samples in order to approximate which elution contained the most protein for the enzyme kinetics assays. Quick Bradford Assays simply determine that protein is

in fact present. For each elution fraction, 5 µL of the elution was mixed with 250 µL of Bradford Reagent. Color change was noted, and then the samples were run at 595 nm. A graph of the absorbency was constructed, but these values were not used to determine concentration. Bradford Assays of each sample were then run at 595 nm following a more extensive protocol so that these values could be measured against standards with known amounts of protein. These values were used to fit a curve of various BSA standards in order to more accurately determine protein concentration in each of the samples.

Enzyme assays were the next step following location of the protein using the gels. The 1mL reaction volume of the conversion of malate to oxaloacetate was run in a 3mL cuvette at 340 nm. The breakdown of NADH was tested, and the reaction was run backwards since equilibrium favors the malate side of the reaction. This allows for the determination of enzyme activity by computing the K_m, V_{max}, and K_{cat} (Fig. 1B). K_m is the concentration of substrate that permits the enzyme to achieve half the maximum reaction rate. V_{max} is the maximum rate of reaction, and this occurs once an enzyme is saturated with substrate. K_{cat} is the turnover number, or the number of substrate molecules each enzyme site converts to product per unit of time. Hyperbolic plots show the relationship between the values, but calculations are done using double reciprocal Lineweaver Burk plots because calculations using the x and y intercepts are more accurate (Fig. 5). Substrate concentration must be varied in order to get the K_m and V_{max} values, so the concentration of oxaloacetate and NADH were varied in the assays.

There were three different enzyme assays for each of the samples following purification. Each reaction was run in a 3mL cuvette with a 1mL reaction volume. Assay 1 was determining the specific activity of the enzyme. In other words, it was determined how much enzyme was

necessary for the reaction to proceed with a change in NADH absorbency of 0.05-0.2 over the course of 60 seconds. Once this necessary volume of enzyme was found, the experiment proceeded to assay 2. In this assay, the concentration of oxaloacetate was varied from 5uM to 250uM in order to determine the K_m value for the oxaloacetate. In assay 3, the concentration of NADH was varied from 20uM to 200uM in order to determine the K_m value for the NADH. In order to complete the assays in which oxaloacetate and NADH were titrated, specific activity had to be established, and this was only possible for the wild type. The entire investigation beginning with streaking the plates from freezer stock BL21 cells and finishing with enzyme kinetics assays was completed twice to verify the reproducibility and accuracy of the data.

Results

To ensure that the desired protein had been induced, cell samples pre and post induction were run in SDS-PAGE gels. This was a checkpoint to make sure that the correct proteins would be purified. When the induced cell samples and the uninduced cell samples from the cultures induced at 37^{o}C were run in 12% SDS-Page gels, it was shown that they had bands slightly below 50 kD. The actual molecular weight of malate dehydrogenase is 32.2 kD (brenda-enzymes), indicating that the purification process was successful (Fig. 6A). Induced and uninduced cell samples from the cultures induced at 25^{o}C were run in a 12% SDS-PAGE gel to determine the desired proteins were purified, and these gels also show that the induced cell samples had bands slightly below 50 kD (Fig. 6B).

Once it was determined that the proteins were accurately expressed, each cell was lysed and added to 6.25mL of Ni-NTA resin and His-Binding buffer in order to bind the His-tagged proteins. Two resin bed volumes (12.5mL) of His-Wash buffer was used to wash the samples for

contamination and unbound protein. One resin bed volume (6.25mL) of His-Elution buffer was used to elute the His-tagged proteins from the resin so they could be used for enzyme assays. The absorbency of the wild type and mutants for each sample was monitored at 280 nm because that is the wavelength at which proteins absorb. Absorbency was monitored for the wash and elution steps each time the buffer was added to the purified resin (Fig. 7).

Once the absorbency for the purifications reached their baseline, meaning there was no more protein to be eluted from the resin, quick Bradford data for each elution showed an approximation of which samples contained the most protein for the kinetics assays. Quick Bradford Assays simply determine that protein is in fact present. Color change was noted upon the addition of Bradford reagent to a small fraction of each elution. Graphs were then constructed as a method to compare each of the samples (Fig. 8). Bradford Assays of each sample were then run at 595nm following a more extensive protocol so that these values could be measured against standards with known amounts of protein. These values were used to fit a curve of various BSA standards in order to more accurately determine protein concentration in each of the samples. This data was then used to fit a curve of various BSA standards in order to more accurately determine protein concentration in each of the samples (Fig. 9).

Enzyme kinetics assays were the next step following the quantification of protein in each of the samples. Kinetics assays are useful in determining the effect of each of the mutations on the enzyme by measuring the enzymes activity with each substrate. The reaction is run backwards, and the breakdown of NADH is tested since equilibrium favors the reverse reaction. Specific activity assays illustrate how much enzyme is necessary for the reaction to proceed. Once that has been determined, running the assays across a range of concentrations for NADH

and oxaloacetate demonstrate how well the enzyme binds to each substrate as the wild type and with each respective mutation. From this data, it is possible to calculate K_m, which outlines in a numerical value the ability of the enzyme to bind to its substrate, V_{max}, the maximum rate at which the reaction proceeds, and K_{cat}, the turnover number for the reaction.

The elutions containing the greatest amount of protein were used for enzyme kinetics assays. First, the specific activity of the wild type MDH2 was determined. Therefore, it was determined how much of the enzyme was necessary for the reaction to proceed with a change in NADH absorbency of 0.05-0.2 over the course of 60 seconds. A volume of 50 µL was found to be the amount of enzyme necessary for this rate of change (Fig. 10). At a concentration of $9.83*10^{-27}$ µg/µL, that means it required $4.91*10^{-25}$ µg of protein to achieve the necessary specific activity to proceed.

In the second assay, the concentration of oxaloacetate was varied from 5 µM to 250 µM in order to determine the K_m and V_{max} values for the oxaloacetate. Titrating the substrate across a range of concentrations gives a more accurate result when determining the affinity of the enzyme for the substrate. A graph of each concentration's absorbance over time was constructed, and subsequently a Lineweaver Burk double reciprocal plot was constructed in order to determine the K_m and V_{max} values. The K_m value is the negative reciprocal of the x-intercept, and this was determined to be 0.029 mM. The V_{max} value is the positive reciprocal of the y-intercept, and this was determined to be 36.76 µM/min. The K_{cat} value is the V_{max}/enzyme concentration, and it was calculated to be 199.78 molecules/minute (Fig. 11).

In assay 3, the concentration of NADH was varied from 20 µM to 200 µM in order to determine the K_m and V_{max} values for the NADH. A graph of each concentration's absorbance

over time was constructed, and subsequently a Lineweaver Burk double reciprocal plot was constructed in order to determine the K_m and V_{max} values. The K_m value was determined to be 47.36 mM, the V_{max} value was determined to be 33.78 μM/min, and the K_{cat} value was calculated to be 183.59 molecules/minute (Fig. 12).

The mutant assays were conducted in the same manner as the wild type. Assay 1 was determining specific activity. For G37R, a range of enzyme concentrations were used in an attempt to get a substantial rate of change that would allow me to proceed to titrating each of the substrates into the enzyme. When trying to determine specific activity, various volumes of the elution containing the enzyme were tested. The concentration of the G37R elutions were $2.89*10^{-25}$ μg/μL in 2019, and $4.34*10^{-27}$ μg/μL in 2020. I tried using up to 300 μL of the enzyme in determining the specific activity. This was ⅓ of the total reaction volume, and there was only 5 mL of each elution available. Therefore, using any greater of an amount would be redundant. It was determined there was not enough activity in the enzyme with the G37R mutation to proceed with titrating the substrates (Fig. 13).

The P133L elution with the greatest concentration of protein in 2019 was $5.40*10^{-26}$ μg/μL, and in 2020 the elution with the greatest concentration of protein contained $5.23*10^{-27}$ μg/μL. A range of enzyme concentrations were used in an attempt to get a substantial specific activity. In both 2019 and 2020, a volume of up to 300 μL was used in an attempt to allow the reaction to run properly. This means that up to $1.62*10^{-23}$ μg of protein was added to the reaction, but there was not enough activity to move forward with titrations of each of the substrates (Fig. 14).

The concentration of P207L elutions were $4.62*10^{-26}$ μg/μL in 2019, and $9.83*10^{-27}$ μg/μL in 2020. A range of enzyme concentrations up to $1.39*10^{-26}$ μg in 300 μL were used in an attempt to get a substantial specific activity. However, no significant activity could be detected either in 2019 or 2020 (Fig. 15). Therefore, the investigation into the kinetics activity of P207L could not proceed.

Since the enzyme kinetics assays did not give much data to use for comparison against the wild type, I proceeded to conduct some *in silico* (computer-based) experiments to further investigate the structural implications of each mutation on the enzyme. Each mutation's FASTA sequence was run through Phyre2, and the results were modeled in Pymol (Fig. 16). These mutations were then overlaid with the wild type structure in order to better compare the structural changes made by each enzyme (Fig. 17). These structures were then processed through H++, a web-based software that predicts how structural changes may impact titration curves. The changes in pKa values of the amino acids surrounding each mutation were then compared with the wild type. There was not a significant difference in pKa values, but there were some slight changes in the residues closer to the mutations (Fig. 18). Therefore, the protonation states of the residues would be altered, and this could affect the interactions between the residues in the enzyme.

Discussion and Conclusions

The protein in each sample was successfully purified each time, and this was supported by the results shown in the SDS-PAGE gels as well as the separate Bradford Assays. The wild type MDH2 sample produced a significant amount of activity, and enzyme kinetics values were able to be generated. The experimental K_m and V_{max} values for oxaloacetate were 0.029 mM and

36.76 μM/min, respectively. The K_{cat} was calculated to be 199.78 molecules/minute. This means that 199.78 molecules are converted to product each minute that the reaction runs until equilibrium is reached. There is not much known about the kinetic parameters of MDH2, so it is difficult to find a "standard" with which I could compare the experimental values. However, a low K_m illustrates high binding affinity, and high V_{max} and K_{cat} values show a substantial rate of reaction.

The K_m value for NADH was calculated to be 47.36 mM. This is a larger value than what was expected, but it is difficult to determine if an error was made since there is not much comparable data. However, the V_{max} value was determined to be 33.78 μM/min, and the K_{cat} value was calculated to be 183.59 molecules/minute. The rate of reaction is similar to that to the oxaloacetate, so there does not appear to be any issues with the binding affinity between the enzyme and substrate.

The most likely explanation for the significant decrease in the activity of the enzymes containing the mutations G37R, P133L, and P207L is that these mutations disrupted the structural integrity of the enzyme. Due to the high specificity of binding between enzymes and their substrates, the mutations killed the activity by making binding extremely difficult. If the enzyme cannot properly bind, then the reaction converting malate to oxaloacetate is not able to move forward. The Kreb's Cycle would subsequently be halted, and a buildup of intermediates would occur. Less NADH would also be produced, so it would not enter other pathways such as the electron transport chain.

It is possible that human error or problems with the freezer stocks played a role in the results. Moving forward, a possible next step would be recovering the plasmids from the freezer

stocks and re-sequencing them. If the stocks became too warm, the cells could have lysed, and they would no longer produce a significant amount of activity. It is also difficult to determine to what degree enzyme activity would be affected *in vivo*. In an *in vitro* study, everything is tightly controlled. However, in the body, the conversion of malate to oxaloacetate could be affected by a myriad of things happening simultaneously in other pathways. Therefore, the data from the *in vitro* study of the enzyme kinetics was unfortunately inconclusive. However, *in silico* experiments were conducted in order to further investigate structural implications of each of the mutations on the enzyme. Another potential issue with the kinetics data is the low enzyme concentration obtained. With better protein expression, activity could be possible for each of the mutations. However, it is not possible to determine this based on the results.

The *in silico* experiments performed to further investigate the results supports this conclusion. When the structures of the mutations were overlaid with the wild type, the structural changes appear to be significant. In order to confirm this, the pKa values of the amino acids surrounding each of the mutations were compared to those in the wild type. While there were not many significant changes (greater than 1), any slight changes could have still affected the protonation state of the residues. This difference in protonation states could have disrupted the integrity within the enzyme structure, or it could have disrupted its interaction with each of the substrates. It is also possible that more charge-charge interactions could be disrupted in the dimer structure of the enzyme. Only the monomer was investigated in H++, but it is possible that residues adjacent to the chain containing the mutation may also be affected.

References

Ait-El-Mkadem, Samira, et al. “Mutations in MDH2, Encoding a Krebs Cycle Enzyme, Cause Early-Onset Severe Encephalopathy.” *The American Journal of Human Genetics,* Cell Press, 15 Dec. 2016 S000292971630492X.

Cascon, Alberto, et al. “Whole-Exome Sequencing Identifies MDH2 as a New Familial Paraganglioma Gene.” *Journal of the National Cancer Institute*, 2015, https://academic.oup.com/jnci/article/107/5/djv053/891892

“Equation: Determine Kcat.” *Graphpad*, 2016, www.graphpad.com/guides/prism/7/curve-fitting/reg_kcat.htm?toc=0&printWindow.

Hock, B. “Mitochondrial Malate Dehydrogenase of Watermelon Cotyledons: Time Course and Mode of Enzyme Activity Changes during Germination.” *SpringerLink*, Springer-Verlag, 1976, link.springer.com/article/10.1007/BF00390909.

Lasserre, Jean-Paul, et al. “Yeast as a System for Modeling Mitochondrial Disease Mechanisms and Discovering Therapies.” *The Company of Biologists,* 2015, http://dmm.biologists.org/content/8/6/509?ct=ct

“Lineweaver–Burk Plot.” *Wikipedia*, Wikimedia Foundation, 7 Feb. 2018, en.wikipedia.org/wiki/Lineweaver%E2%80%93Burk_plot.

“Lineweaver-Burk Woes.” *Lineweaver-Burk Woes. - Biology Biochemistry*, ask.metafilter.com/32682/Lineweaverburk-woes.

L., Nealson David, et al. *Lehinger, Principles of Biochemistry*. W.H. Freeman and Company, 2008.

Remacha, Laura, et al. “Targeted Exome Sequencing of Krebs Cycle Genes Reveals Candidate Cancer Predisposing Mutations in Pheochromocytomas and Paragangliomas.” *Clinical Cancer Research*, American Association for Cancer Research, 1 Jan. 2017, clincancerres.aacrjournals.org/content/early/2017/07/18/1078-0432.CCR-16-2250.

Rouzier, Cecile, et al. “MFN2 Gene Is Responsible for Mitochondrial DNA Instability and Optic Atrophy 'plus' Phenotype.” *OUP Academic*, Oxford University Press, 20 Dec. 2011, academic.oup.com/brain/article/135/1/23/328725.

“Search KM Value [MM].” BRENDA, www.brenda-enzymes.org/search_result.php?

SIB Swiss Institute of Bioinformatics. “SIB Swiss Institute of Bioinformatics.” *ExPASy*, web.expasy.org/cgi-bin/protparam/protparam1?P40926@noft@.

“Tag-Protein Purification Kit & Gel.” *Tag-Protein Purification Kit & Gel | MBL Life Science -JAPAN-*, ruo.mbl.co.jp/bio/e/product/tag/pickup/tag_purification.html.

Takahashi-Íñiguez, Tóshiko, et al. “Function, Kinetic Properties, Crystallization, and Regulation of Microbial Malate Dehydrogenase.” *Journal of Zhejiang University. Science. B*, Zhejiang University Press, Apr. 2016, www.ncbi.nlm.nih.gov/pmc/articles/PMC4829630/.

“Takara Bio-Home.” *Takara Bio-Home*, www.takarabio.com/.

“Thebuddychemists.” *Thebuddychemists*, thebuddychemists.wordpress.com/.

“The Effect of Substrate Concentration on Enzyme Activity.” *Ucl.* www.ucl.ac.uk/~ucbcdab/enzass/substrate.htm

"The Krebs Cycle - Harnessing Chemical Energy for Cellular Respiration." *Sigma Aldrich*, www.sigmaaldrich.com/technical-documents/articles/biofiles/citric-acid-cycle.html.

Figures and Tables

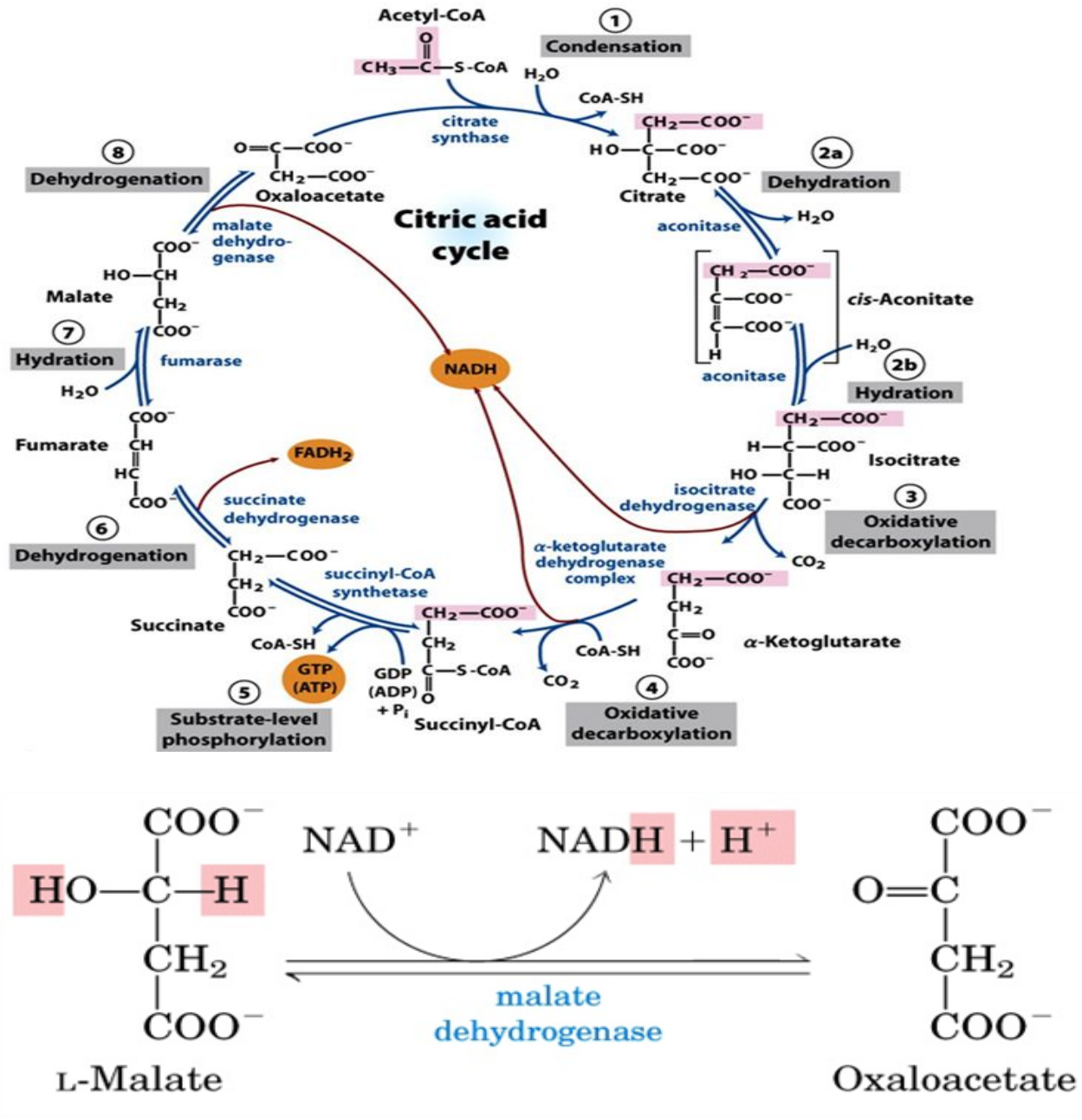

Figure 1 - The Krebs Cycle A) The Krebs Cycle occurs in the mitochondria, generating electron carriers that move to other pathways. *thebuddychemists.wordpress.com* B) The reaction of malate to oxaloacetate as part of occurs at step 8, generating NADH as a byproduct. *Lehinger Principles of Biochemistry*, Sixth Edition

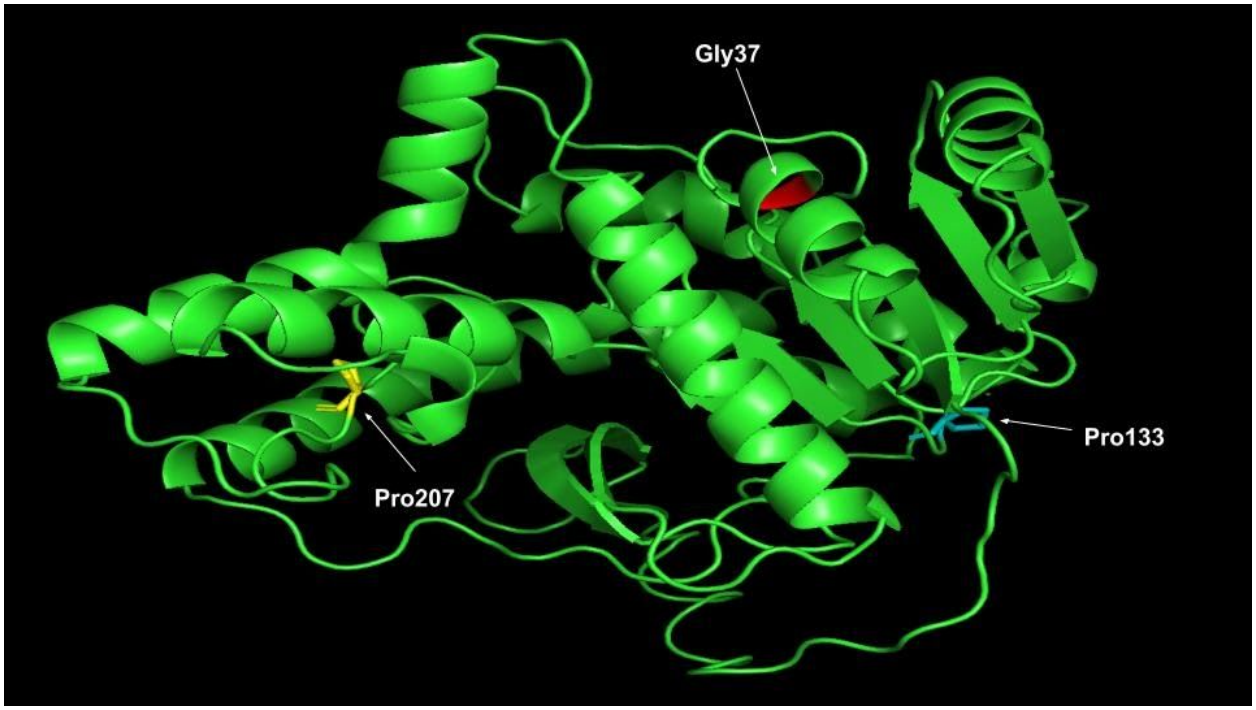

Figure 2 - Locations of Gly37, Pro133, and Pro207 in Wild Type MDH2 as modeled in Pymol

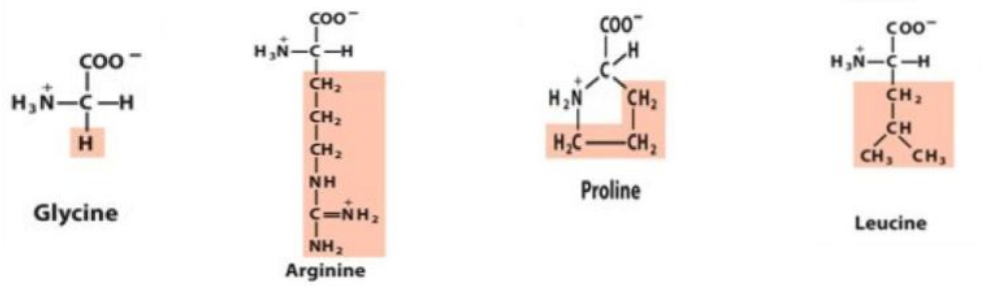

Figure 3 - Structures of glycine, arginine, proline, and leucine.

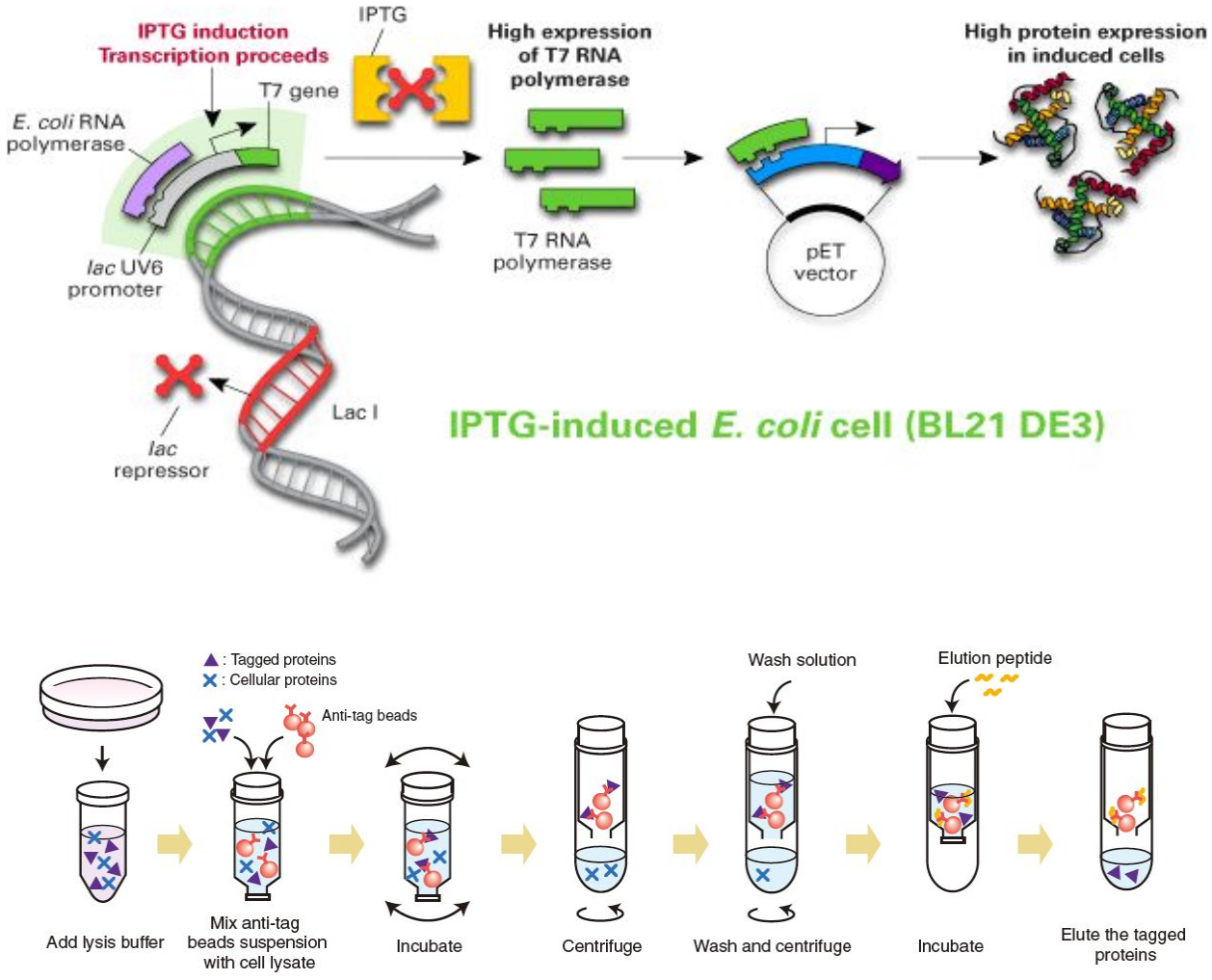

Figure 4 - A**) IPTG inducible protein expression in BL21 DE3 *E. coli* cells** IPTG allosterically binds to the lac repressor, allowing the transcription of genes in the lac operon *takarabio.com* B) **Process of expressing and purifying His-tagged proteins** His-tags are strings of histidine residues with a high affinity for metal ions, such as nickel. The nickel in the resin binds the his-tagged proteins so they stay on the column during purification. *ruo.mbl.co.jp*

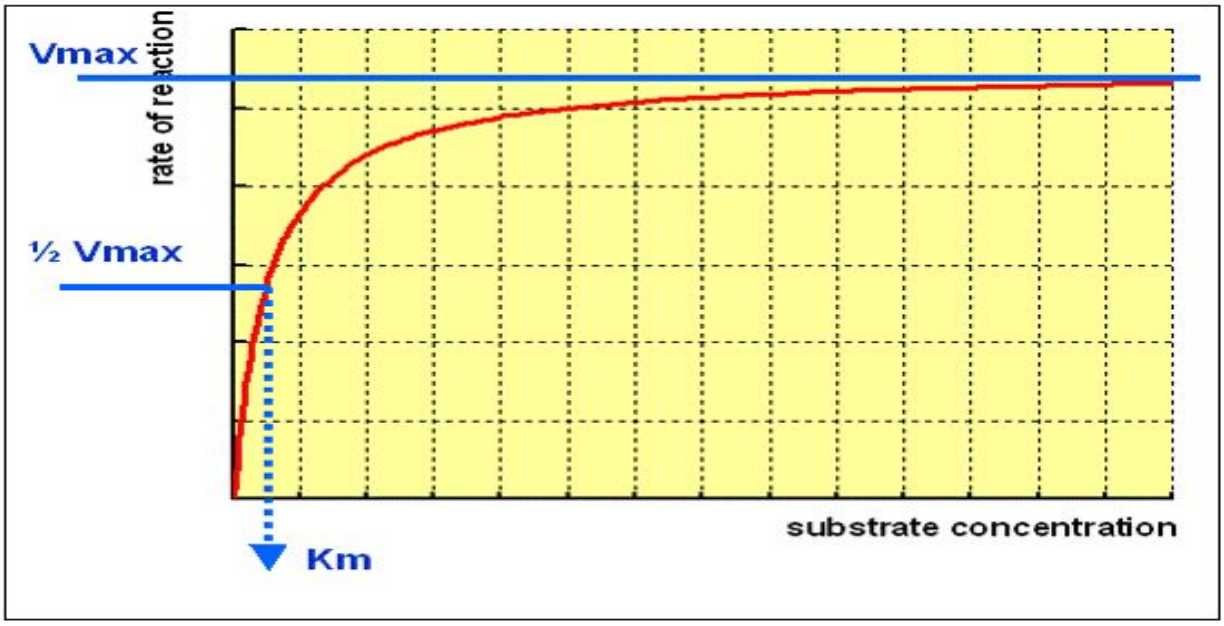

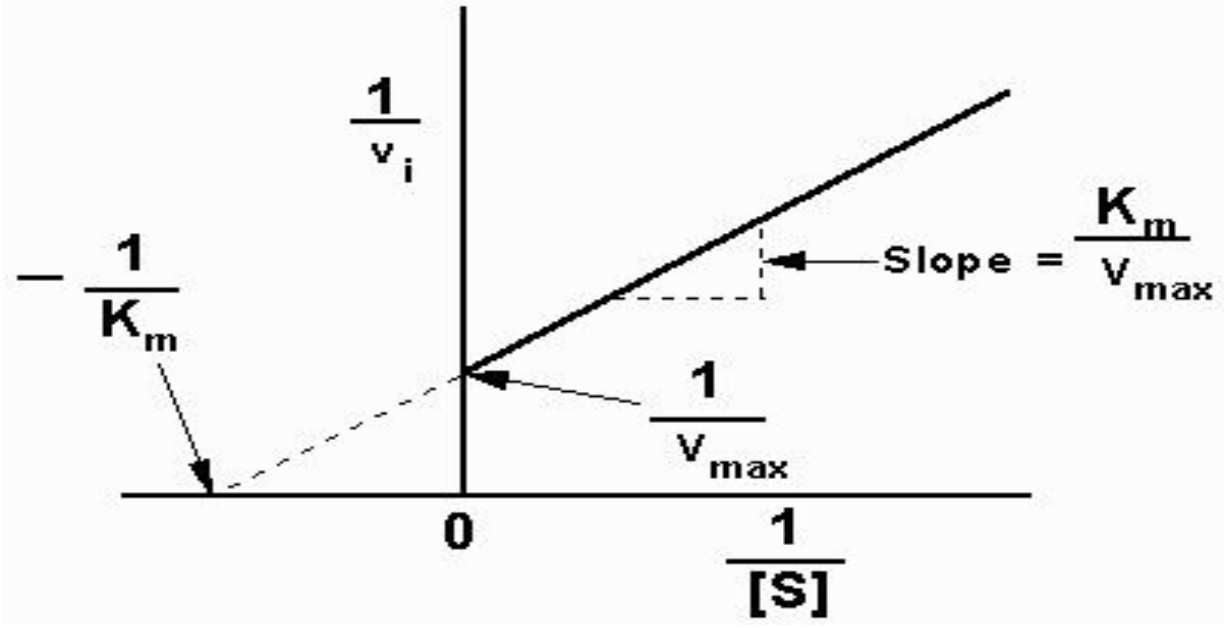

Figure 5 - Determining K_m and V_{max} on a graph A)The hyperbolic relationship between reaction rate and substrate concentration shown on a graph with K_m and V_{max} values where appropriate. "Equation: Determine K_{cat}." *Graphpad, 2016* B) The double reciprocal Lineweaver Burk plot illustrates the relationship of K_m and V_{max} in quantitative analysis. *ask.metafilter.com*

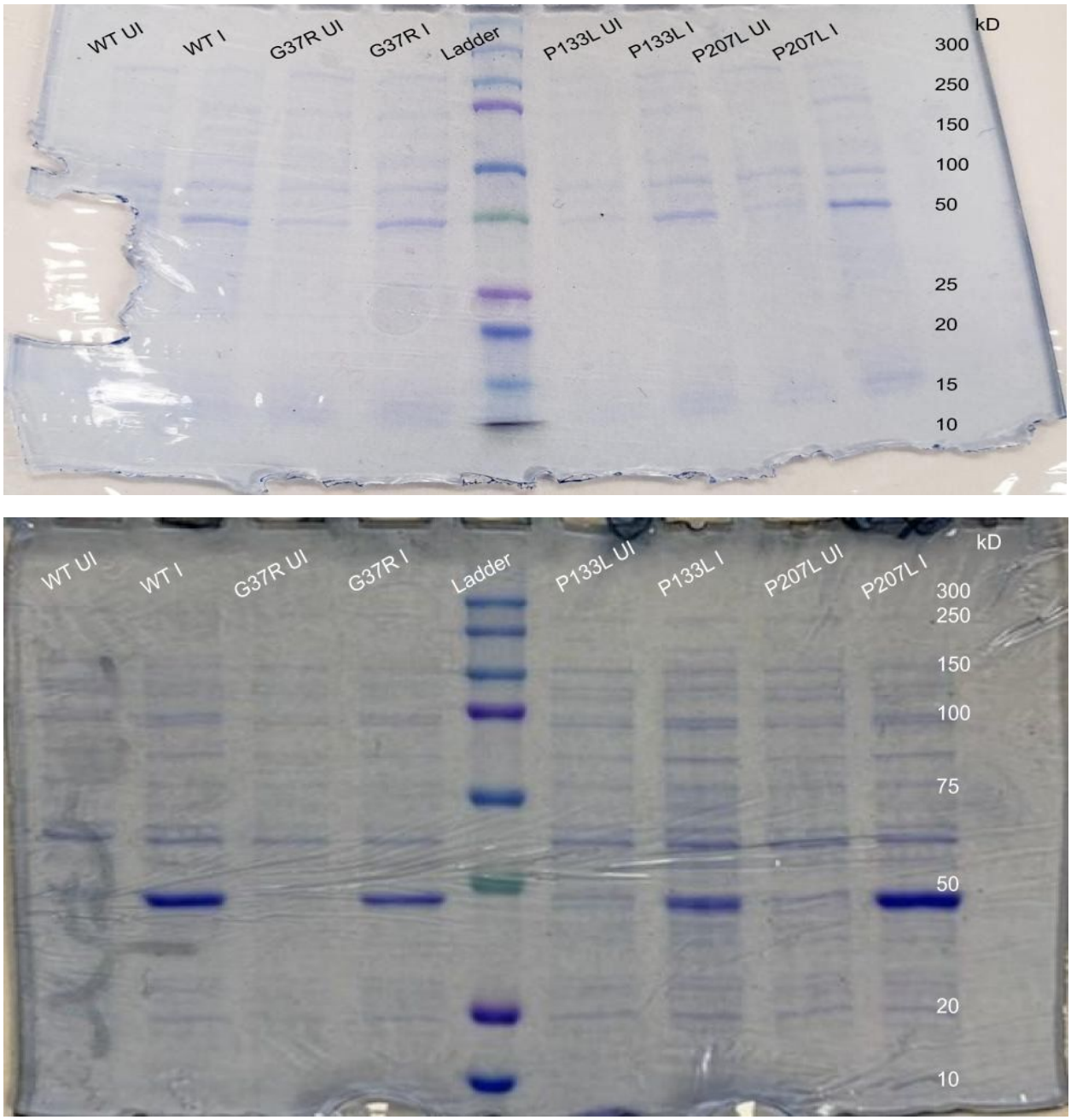

Figure 6 - Coomassie Gel of MDH2 Induction A) Samples induced at 37ºC in 2019 were run against their complementary uninduced samples on a 12% SDS-PAGE gel to verify that the desired protein was expressed, and B) Samples induced at 37ºC in 2020 were run against their complementary uninduced samples on a 12% SDS-PAGE gel to verify that the desired protein was expressed. Wild Type is denoted WT, and the mutations are denoted as G37R, P133L, and P207L, with the final letter defining the mutation. Uninduced is shown as UI, and Induced is shown as I.

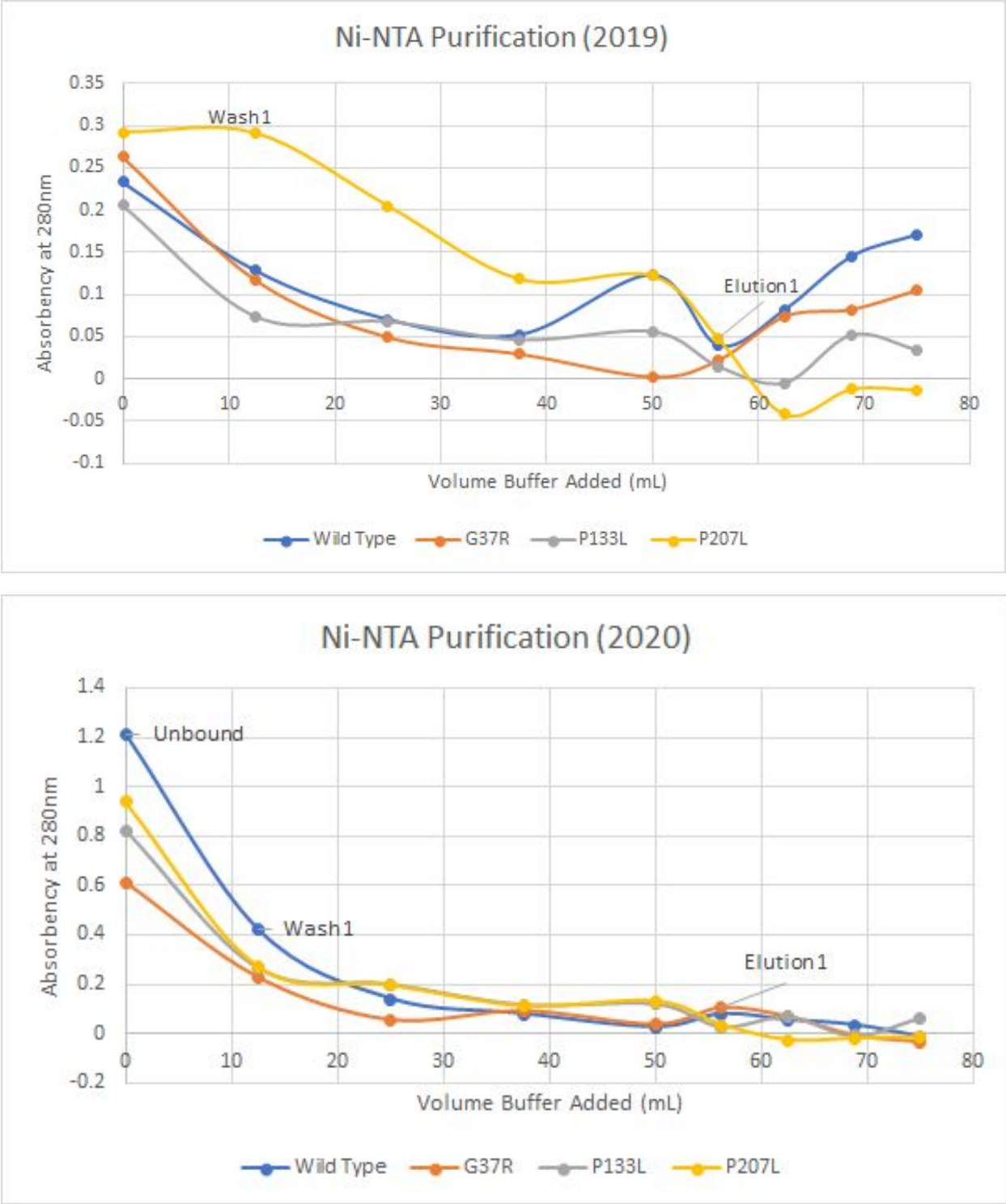

Figure 7 - Ni-NTA Purification Data Absorbency values of the His-Wash and His-Elution of the induced cell pellets in A) 2019 and B) 2020

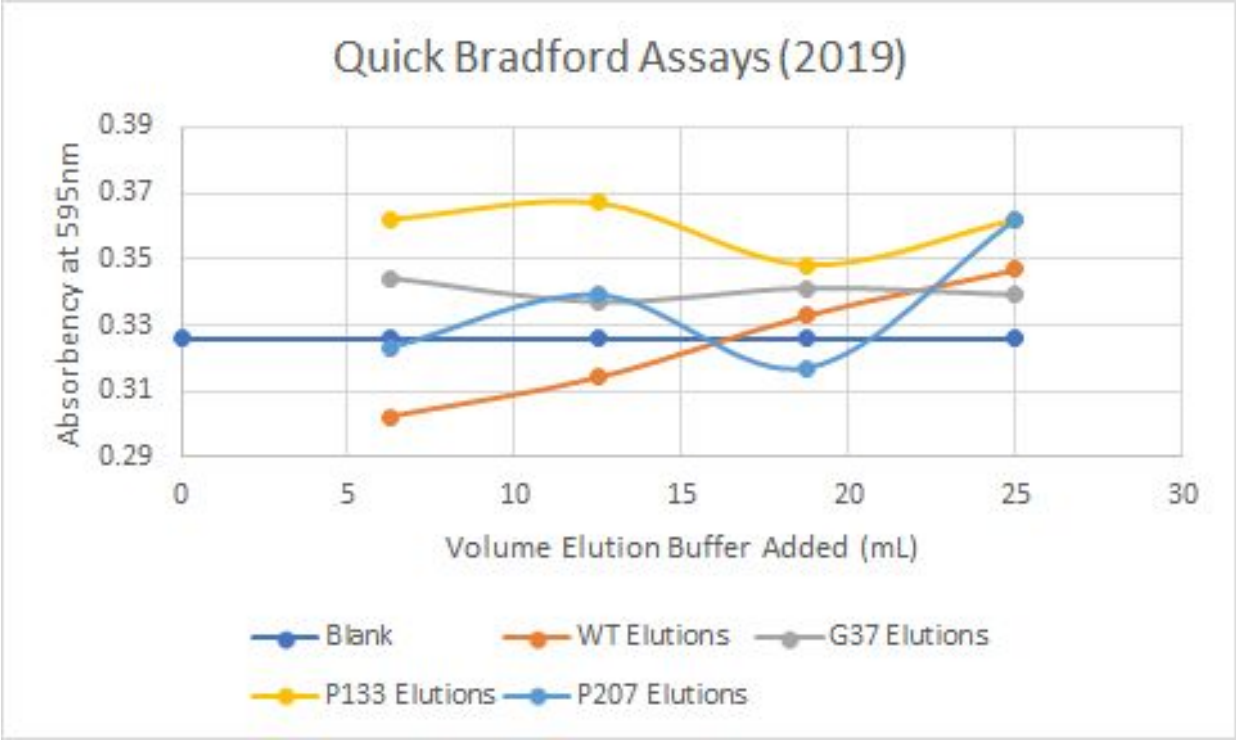

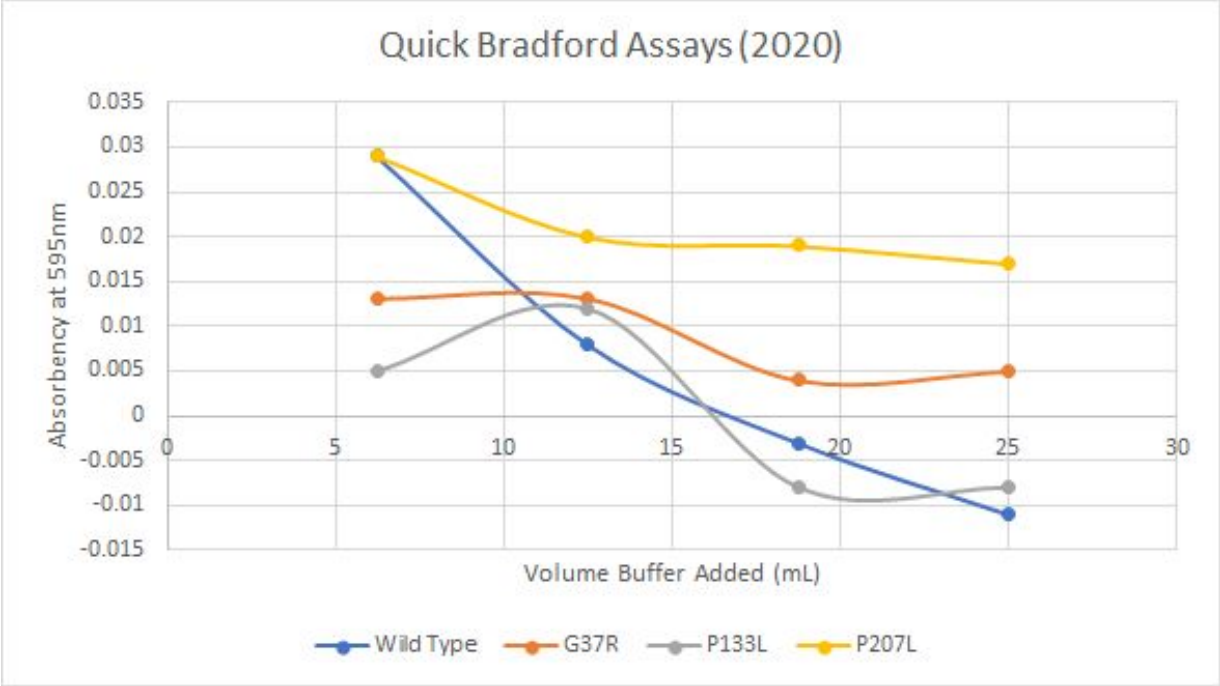

Figure 8 - Quick Bradford Data A) Quick Bradford Assays of Elutions show approximately how much protein is contained in each sample based on its absorbance at 595 nm (2019) B) Quick Bradford Assays of Elutions show approximately how much protein is contained in each sample based on its absorbance at 595 nm (2020)

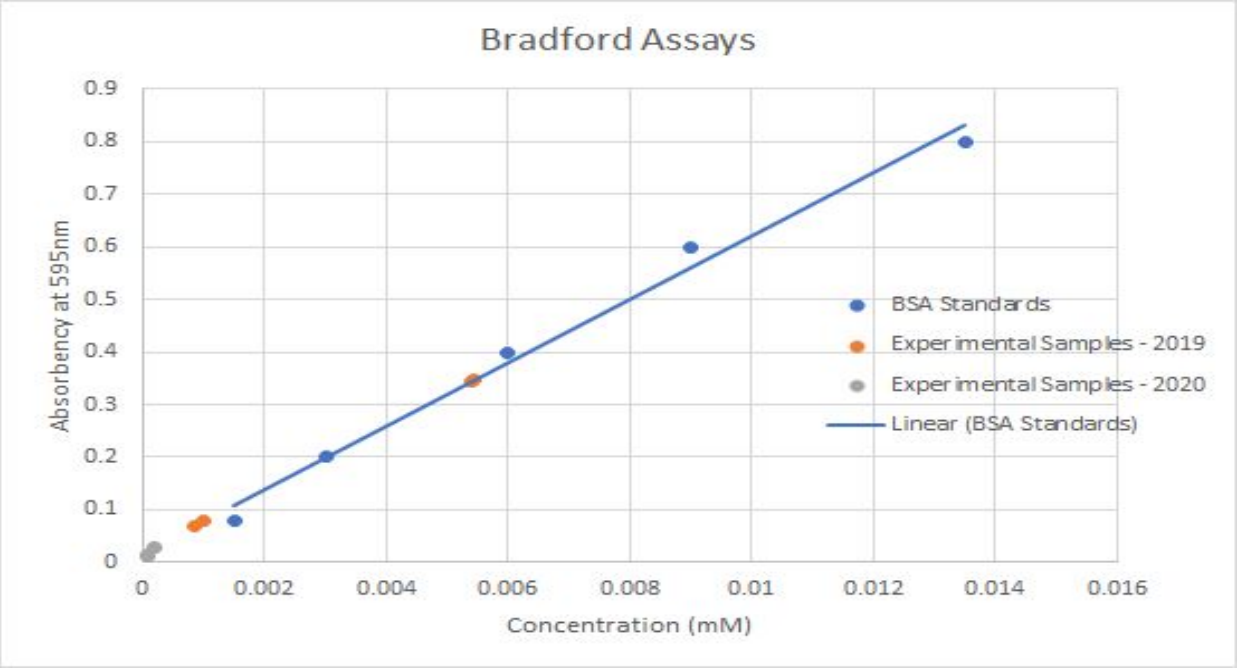

Sample	Absorbance (595 nm)	Calculated Concentration (µM)
Wild Type Elution 4	0.347	5.46
G37R Elution 1	0.344	5.41
P133L Elution 2	0.079	1.01
P207L Elution 4	0.07	0.864

Sample	Absorbance (595 nm)	Calculated Concentration (µM)
Wild Type Elution 1	0.029	0.184
G37R Elution 1	0.013	0.0812
P133L Elution 2	0.012	0.0978
P207L Elution 1	0.029	0.184

Figure 9 - Protein Concentration in Each Sample Based on Bradford Assay A) Graph of Bradford Assays of the elutions used in the kinetics assays plotted against BSA standards in order to determine their absorbencies in 2019 and 2020. B) Table of calculated protein concentration in each sample based on the equation produced from the BSA standards in 2019 and C) 2020

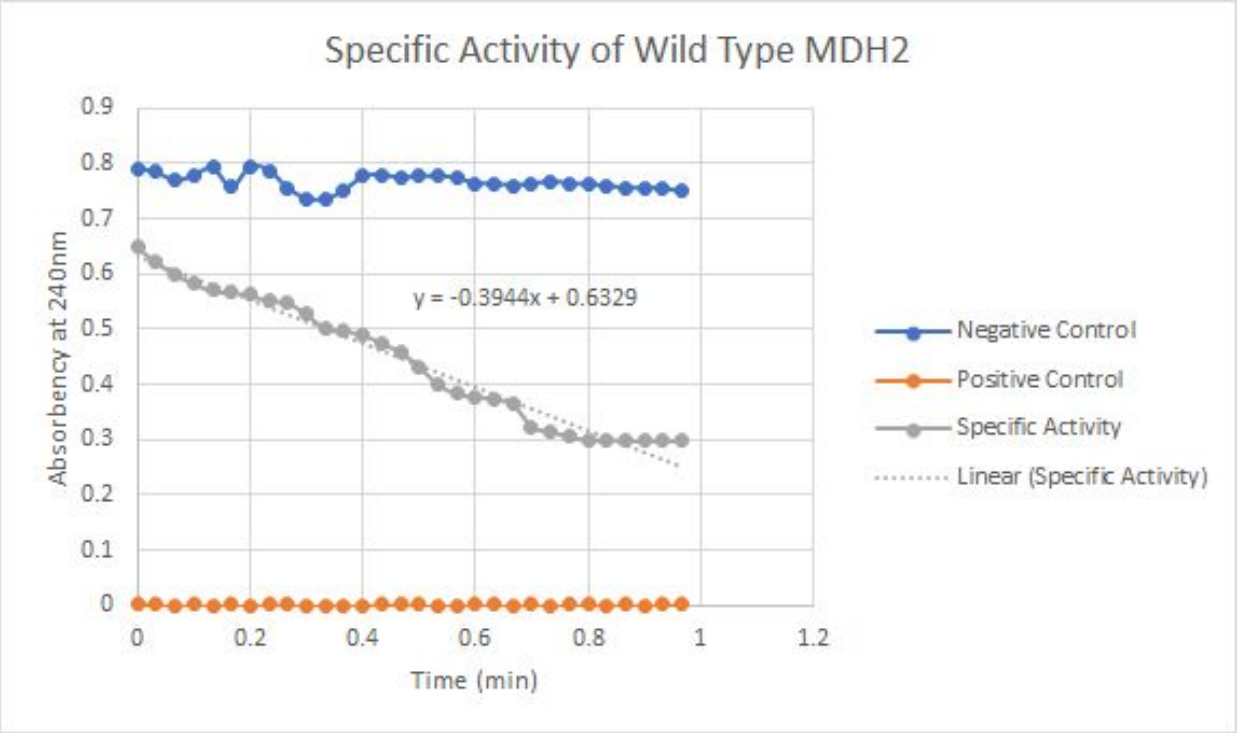

Figure 10 - Specific Activity of Wild Type MDH2 The specific activity curve for the wild type shows that $4.92*10^{-25}$ µg of the enzyme was necessary for a rate of change of 0.3944.

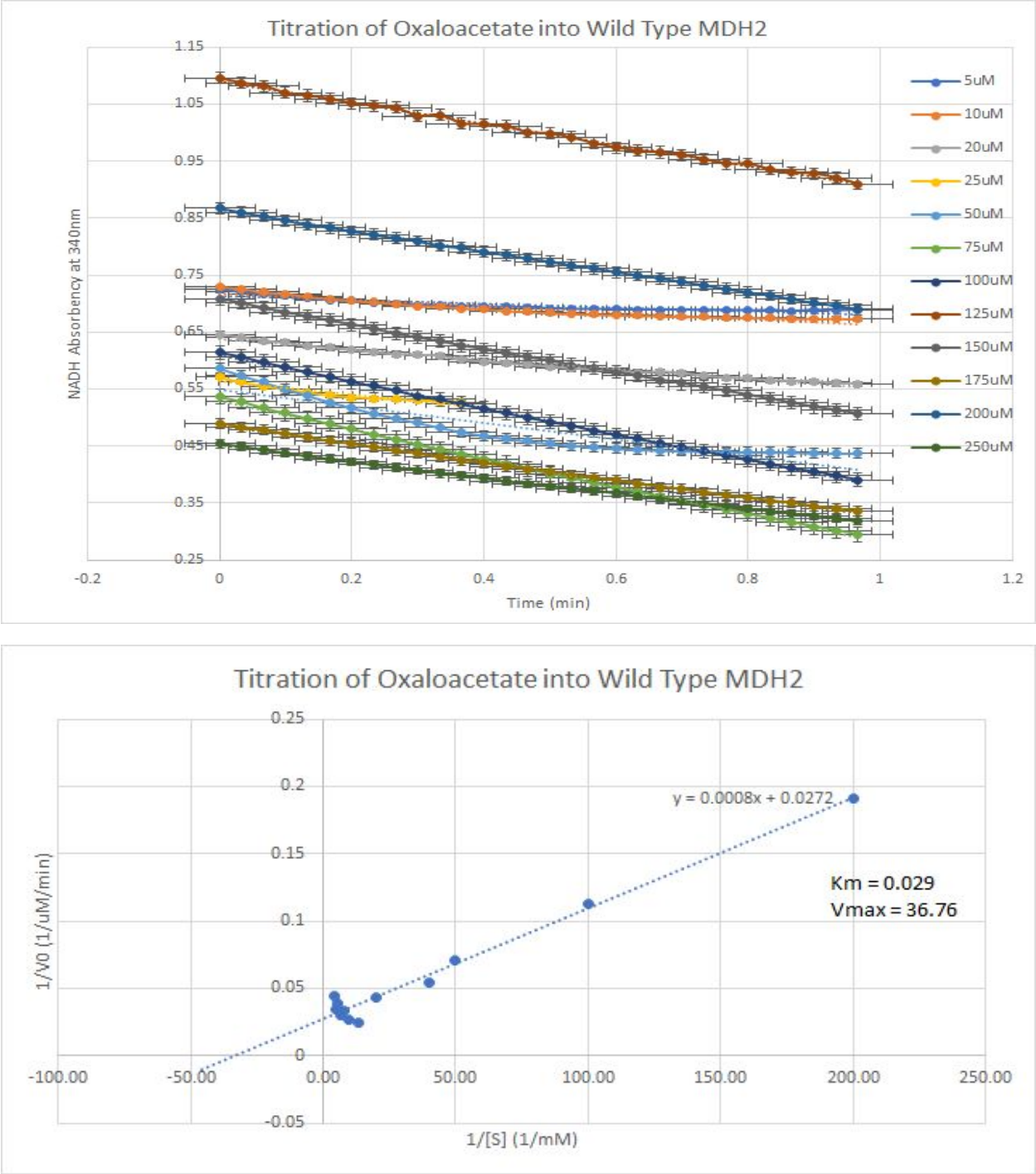

Figure 11 - K_m, V_{max}, and K_{cat} for Oxaloacetate A) NADH absorbency at 340nm is shown over the course of one minute for each of the concentrations of oxaloacetate used in the course of the investigation. Standard error bars are shown to account for major deviations in the data. B) A reciprocal plot of substrate concentration [S] vs velocity (V_0) shows K_m = 0.029 mM, V_{max} = 36.76 µM/min, and K_{cat} = 199.78 molecules/min.

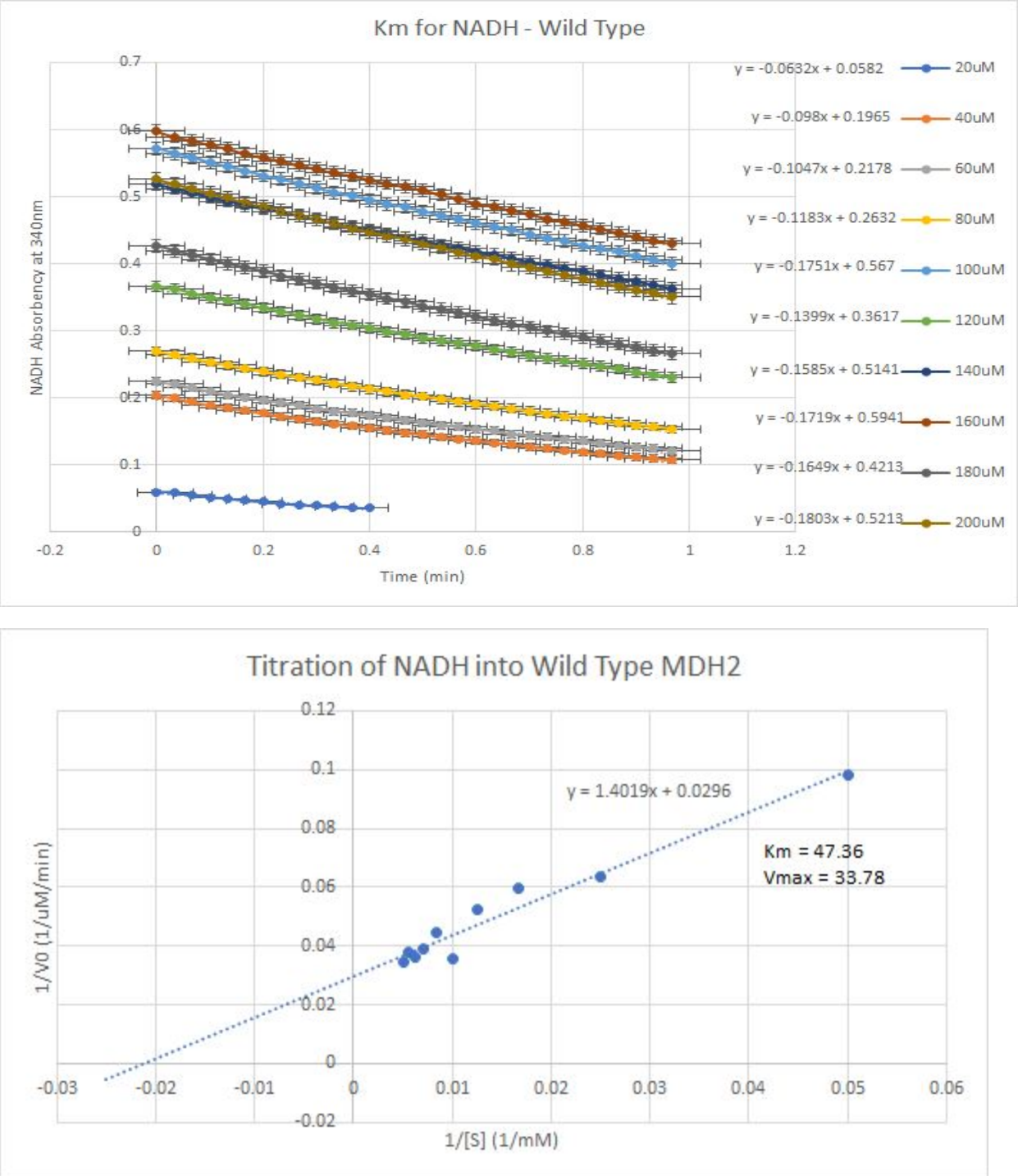

Figure 12 - K_m for NADH - A) NADH absorbency at 340nm is shown over the course of one minute for each of the concentrations of NADH used in the course of the investigation. Standard error bars are shown to account for major deviations in the data. B) A reciprocal plot of substrate concentration [S] vs velocity (V_0) shows K_m = 47.36 mM, V_{max} = 33.78 µM/min, and K_{cat} = 183.59 molecules/min.

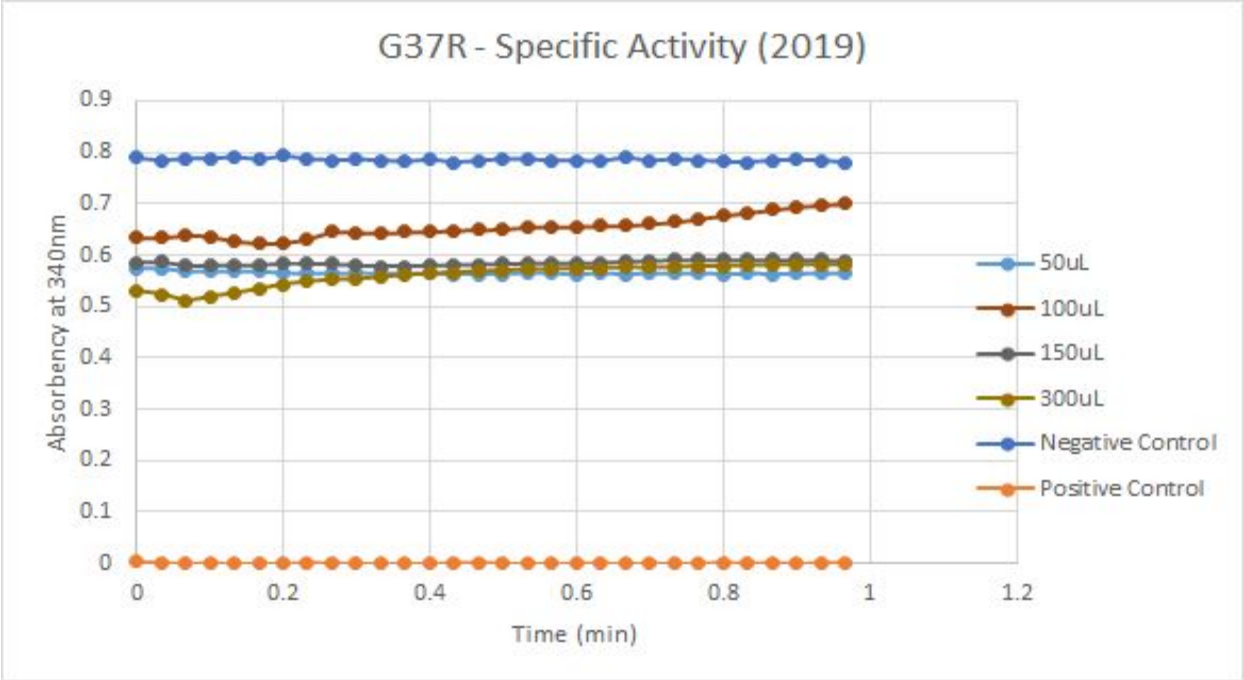

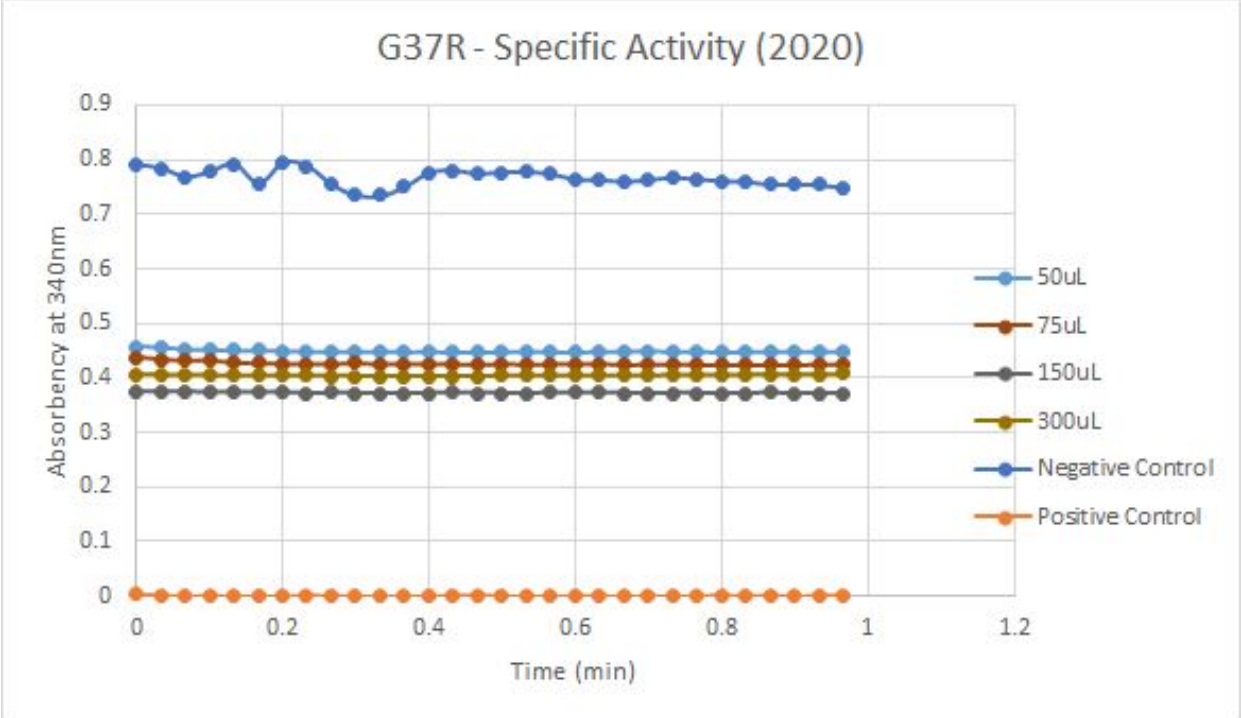

Figure 13 - Specific Activity of G37R The specific activity of G37R was monitored against a positive and negative control in order to determine the activity of the enzyme. Unfortunately, no significant activity could be recorded during investigations in A) 2019 or B) 2020.

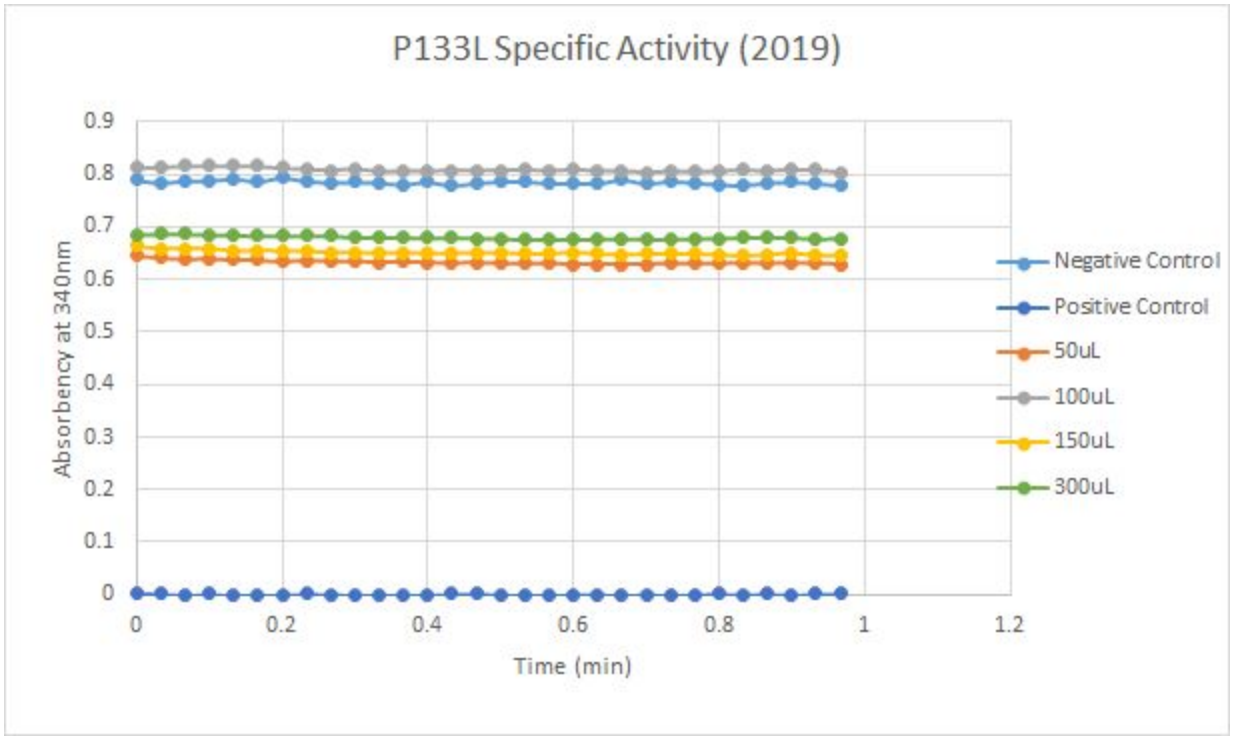

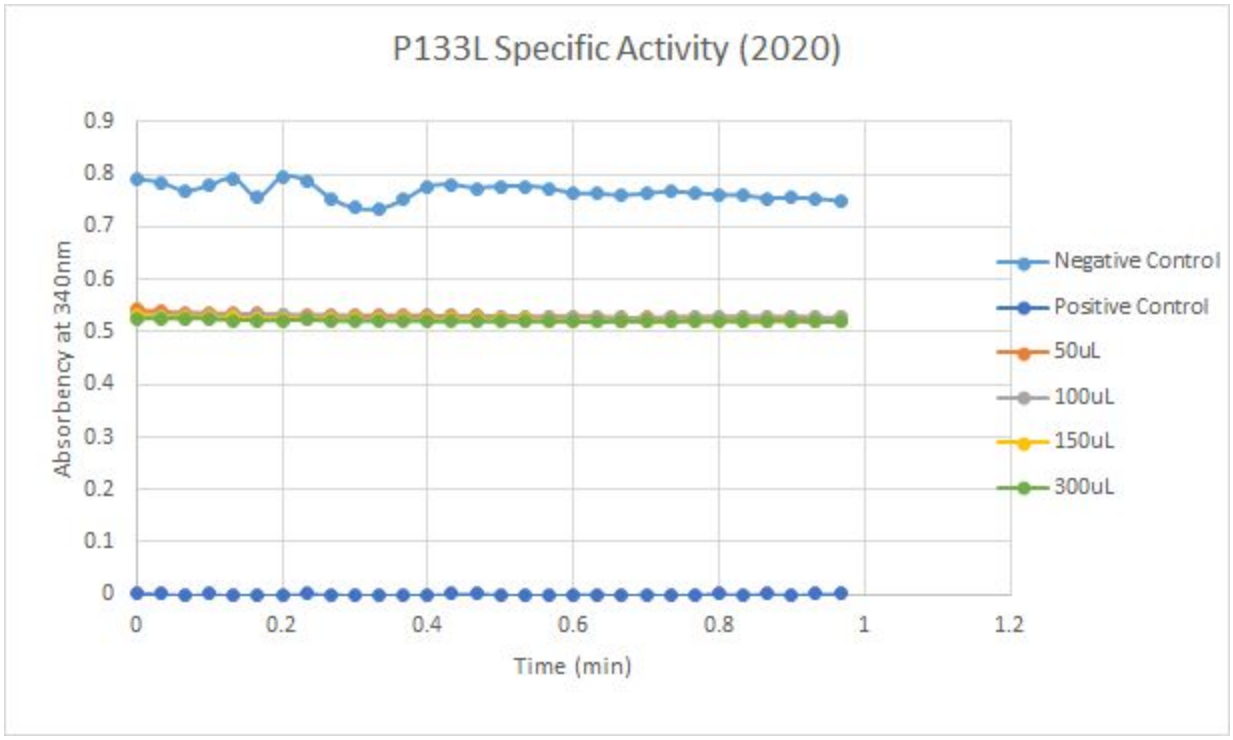

Figure 14 - Specific Activity of P133L The specific activity of P133L was monitored against a positive and negative control in order to determine the activity of the enzyme. Unfortunately, no significant activity could be recorded during investigations in A) 2019 or B) 2020.

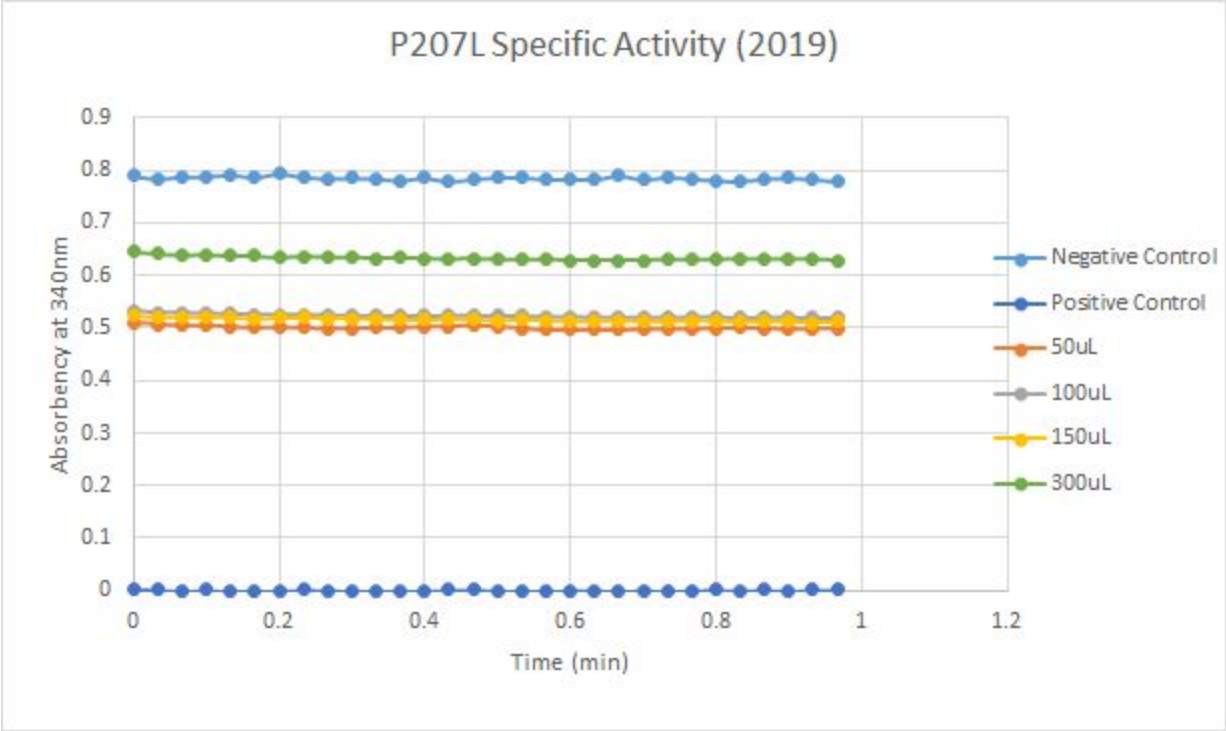

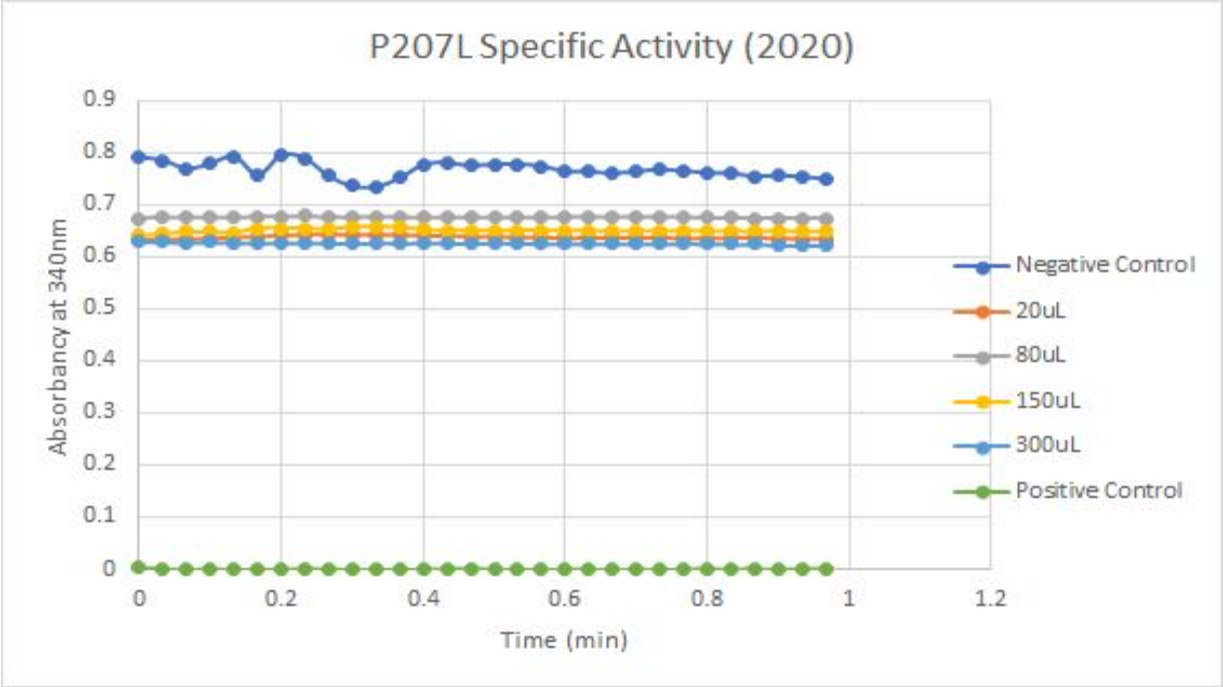

Figure 15 - Specific Activity of P207L The specific activity of P207L was monitored against a positive and negative control in order to determine the activity of the enzyme. Unfortunately, no significant activity could be recorded during investigations in A) 2019 or B) 2020.

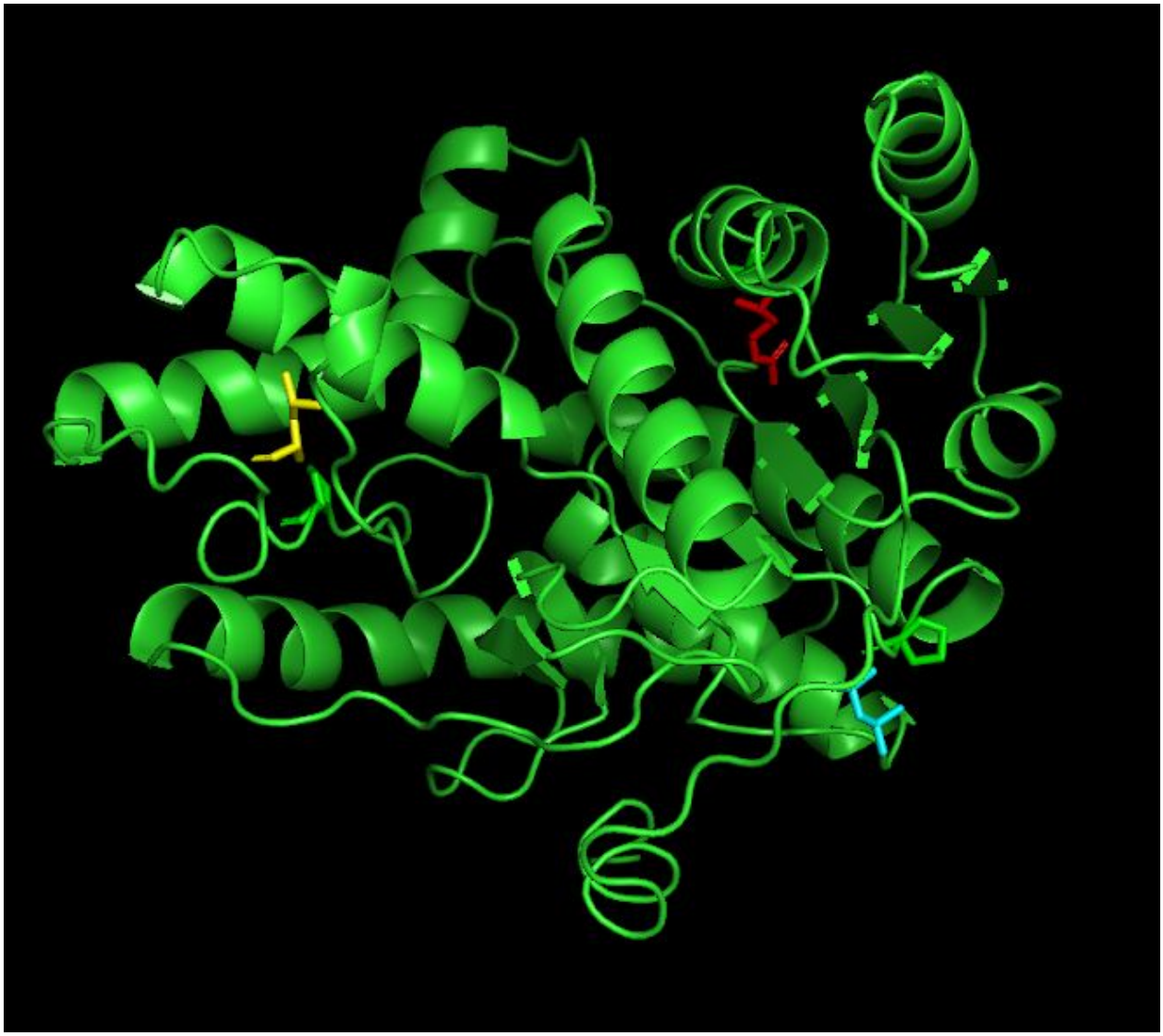

Figure 16 - Phyre2 Mutant Structures modeled in Pymol Each of the mutations were modeled in Pymol using the results from Phyre2. G37R is red, P133L is blue, and P207L is yellow.

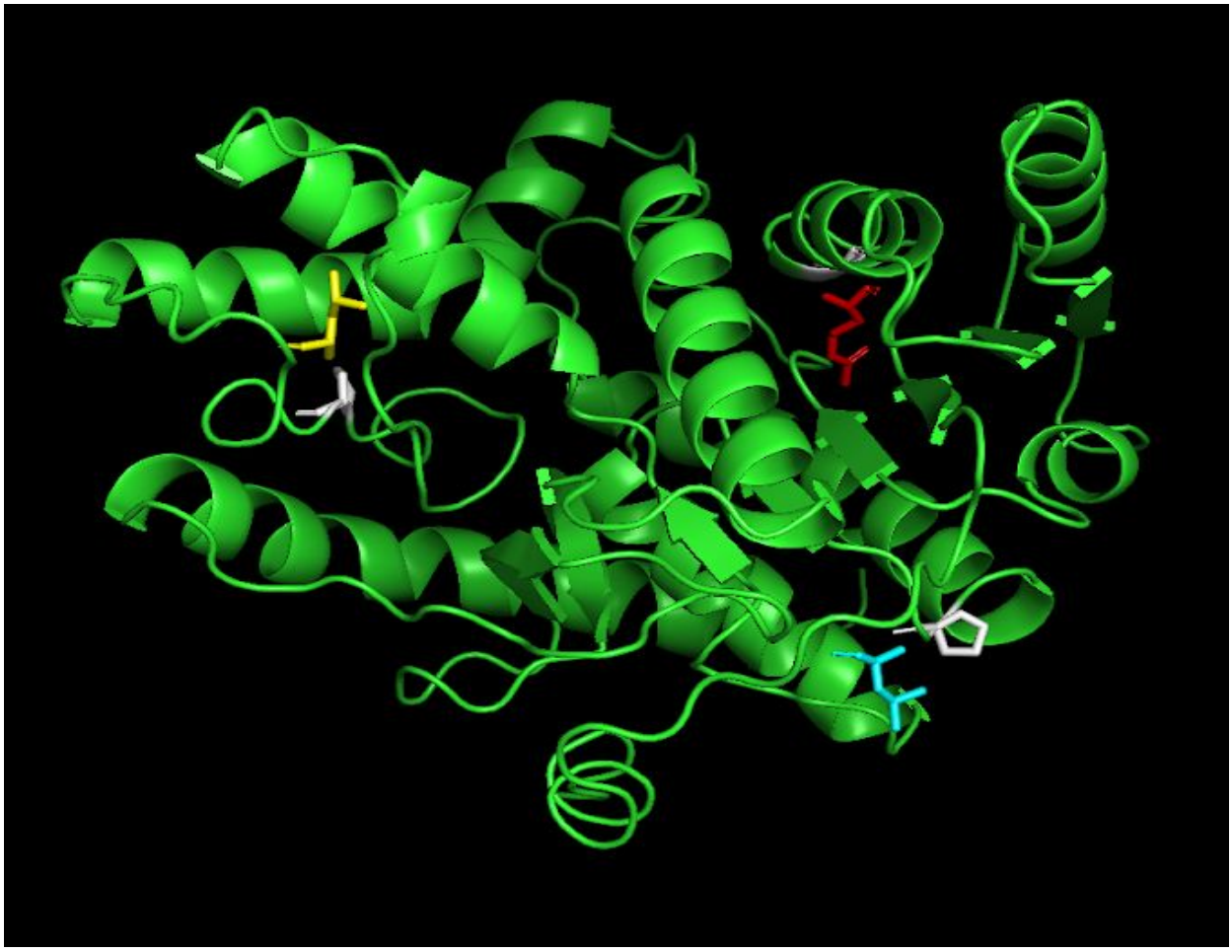

Figure 17 - Mutant Structures Overlayed with the Wild Type Structures The G37R mutation (red) was overlaid with the wild type (white). The P133L mutation (blue) was overlaid with the wild type (white). The P207L mutation (yellow) was overlaid with the wild type (white).

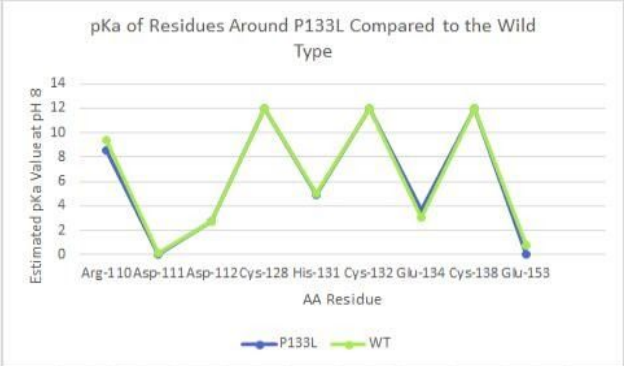

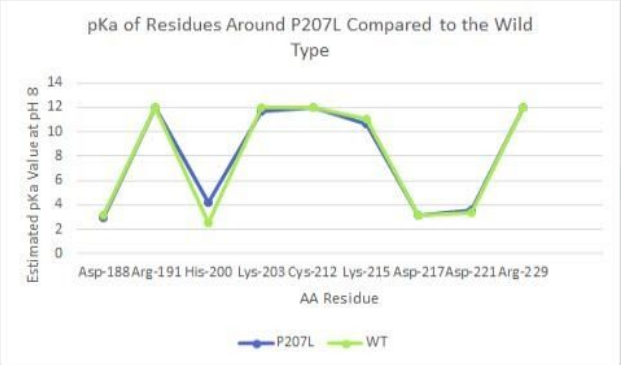

	WT	G37R
N-term	6.7	7.1
Arg-7	12	12
Arg-14	12	12
Arg-15	12	12
Lys-26	11.1	12
Arg-37		10.8
Lys-45	12	10.7
Arg-52	12	12
Tyr-56	12	12
Asp-57	1.4	0.1

	WT	P133L
Arg-110	9.4	8.5
Asp-111	0.1	0
Asp-112	2.7	2.7
Cys-128	12	12
His-131	5	4.9
Cys-132	12	12
Glu-134	3	3.7
Cys-138	12	12
Glu-153	0.8	0

	WT	P207L
Asp-188	3.1	2.9
Arg-191	12	12
His-200	2.5	4.2
Lys-203	12	11.7
Cys-212	12	12
Lys-215	11.1	10.6
Asp-217	3.1	3.1
Asp-221	3.3	3.6
Arg-229	12	12

Figure 18 - The pKa values of the amino acids surrounding each mutation are compared with the wild type.